FISEVIER

Contents lists available at ScienceDirect

Journal of Physics and Chemistry of Solids

journal homepage: www.elsevier.com/locate/jpcs



Lattice dynamics and electronic Grüneisen parameters of femtosecond laserexcited bismuth



A. Bugayev^a, H.E. Elsayed-Ali^{a,b,*}

- Applied Research Center, Old Dominion University, Newport News, VA, 23606, USA
- ^b Department of Electrical and Computer Engineering, Old Dominion University, Norfolk, VA, 23529, USA

ARTICLE INFO

Keywords:
Bismuth
Coherent acoustic phonon
Electronic Grüneisen parameter
Femtosecond laser heating
Hot electron blast

ABSTRACT

In this study, we probed the lattice dynamics of bismuth subjected to femtosecond laser irradiation by ultrafast electron diffraction. The changes in the diffraction intensity and angle were determined. The lattice exhibited compression upon laser excitation, followed by expansion with damped vibrations. Coherent acoustic phonons were observed as oscillations in the lattice spacing. The results were analyzed using a damped harmonic oscillator model where the hot electrons caused the blast compressive force, which resulted in lattice-spacing oscillation for the expanded lattice following the compression. We obtained the rate of electron–phonon coupling, its anisotropy, and the Grüneisen parameters of the electronic subsystem.

1. Introduction

Ultrafast electron diffraction (UED) is a pump-probe technique where an electron pulse synchronized with a laser pulse is used to determine the transient structural dynamics initiated by the laser interacting with the sample under investigation. UED is an established tool for the direct observation of phase transitions in metals and semiconductors, reactions at surfaces and interfaces, phonon dynamics, isolated chemical reactions in molecular beams, photochemical processes in organics, intermolecular electron transfer, and metal-to-metal electron transfer [1–4]. Since the early study by Williamson et al. using 20-ps time-resolved electron diffraction to probe the melting of an aluminum thin film [5], the temporal resolution of this technique has been extended to a few hundred femtoseconds [6,7].

Bismuth was previously studied by UED to observe coherent acoustic phonon oscillations [8], probe its solid–liquid phase transition on a sub-vibrational time scale [9], and determine the anisotropy of the electron–phonon energy coupling in Bi [10,11]. In the present study, we conducted a UED experiment where the diffraction intensity and angle were probed after excitation with a femtosecond laser pulse. The observed damped oscillations in the lattice spacing are described by a model where the hot electron blast force is followed by coherent acoustic phonons. We also determined the energy exchange rate based on electron–phonon coupling and the electronic Grüneisen parameter.

2. Experimental approach

In our UED-based study of the lattice dynamics of Bi films, laser pulses with a pulse width of ~110 fs, wavelength of 800 nm, and a repetition rate of 1 kHz were used to excite the sample. Both the intensity and angle of diffraction orders were probed. The sample was a Bi thin film with a thickness of 20-22 nm, which was thermally evaporated on a carbon-coated (carbon thickness < 15 nm) transmission electron microscopy (TEM) copper grid (hole size $\sim 42 \,\mu\text{m}$). The deposition rate and final Bi film thickness were measured with a crystal thickness monitor. The absolute calibration of the crystal thickness monitor was performed by comparing its final thickness measurement with that obtained from a cross-sectional scanning electron microscopy image of Bi evaporated on a silicon wafer, which was placed at the same location as the TEM grids. The photoactivated electron gun and pumpprobe setup used in the experiment were described previously [12,13]. The electron gun produced 35-keV electron pulses with a pulse width of \sim 1.3 ps at the sample location. The electron pulse width increased with the laser fluence used to excite the photocathode. To maintain the electron pulse width at ~ 1.3 ps, the excitation laser fluence on the photocathode was kept constant throughout the described experiments. A movable Faraday cup was used to measure the average electron current and the numbers of electrons per pulse were obtained. The number of electrons per pulse was ~5000 under the experimental conditions employed. The 800-nm pump fluence on the sample was $\sim 1.5 \text{ mJ/cm}^2$. The melting threshold of Bi is 2.85 mJ/cm^2 . Fig. 1 shows

^{*} Corresponding author. Applied Research Center, Old Dominion University, Newport News, VA, 23606, USA. *E-mail address*: helsayed@odu.edu (H.E. Elsayed-Ali).

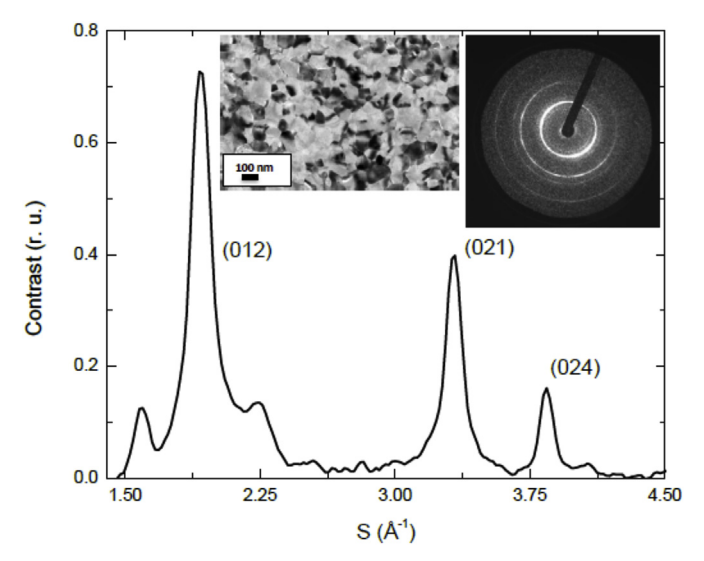


Fig. 1. Radial averaged profile of the diffraction intensity determined for the polycrystalline Bi film as a function of the momentum transfer $S=2\pi/d$ (d is the interplanar distance). Insets show a TEM image and diffraction pattern for the Bi film.

the UED pattern obtained for the Bi film and its radially averaged profile. Bismuth has a rhombohedral crystal structure with the space group $R\bar{3}m$. We used the hexagonal notation for identifying the diforders, where $a = b = 50.455 \,\text{nm}$, $c = 51.186 \,\text{nm}$, $\alpha = \beta = 90^{\circ}$, and $\gamma = 120^{\circ}$. The two side peaks around the (012) order were separated from the (012) peak by a similar angle, thereby indicating the presence of systematic defects in the grains such as misfit dislocations. These satellite peaks are often observed in electron and Xray diffraction patterns [14]. The TEM image of the Bi sample shown in the inset in Fig. 1 indicated that the sample comprised a flat polycrystalline film with a grain size in the order of several tens of nanometers. The diffraction patterns were captured with delay steps of 1 ps for delay ranges of -1 ps $\leq t \leq 3$ ps and 1.5 ps for ≥ 3 ps. Each timeresolved electron diffraction pattern was acquired twice and the average value was used in the analysis. The accuracy of the diffraction angle measurement was determined based on the standard deviation of the diffraction's radius measured at different delay times without excitation, where it was calculated as 1.1×10^{-4} .

3. Results and discussion

Fig. 2 shows the time-resolved intensity contrast $(I(t) - I_0)/I_0$ in relative units and the percentage change in the radius $(R(t) - R_0)/R_0$ (%) for the diffraction orders, where I(t) and R(t) are the intensity and radius of the diffraction orders at time t, respectively, and I_0 and R_0 are the unperturbed (at the time before the laser pulse arrived at the target) values of the diffraction intensity and radius. Several important features are apparent after comparing the temporal changes in the contrast and radius. First, the Bragg peak positions exhibited a damping quasi-oscillatory motion, which was centered at a newly established position with a reduced radius and a time period of 7-10 ps. In addition, the temporal dependences of the intensity contrast for diffraction orders I(t) exhibited less distinct oscillatory behavior in terms of the amplitude. A phase correlation was not observed between I(t) and R(t), which indicates that the effects of lattice distortion observed according to the changes I(t) and R(t) were not directly dependent on each other. For the (021) and (024) diffraction orders, the dynamics of the R(t) dependence started with a positive change (compression) shortly after the zero delay-time, which transformed into a negative change (expansion) as the delay time increased. The time period during which the change in R(t) exhibited compression was about 2.5-3.5 ps (for diffraction orders

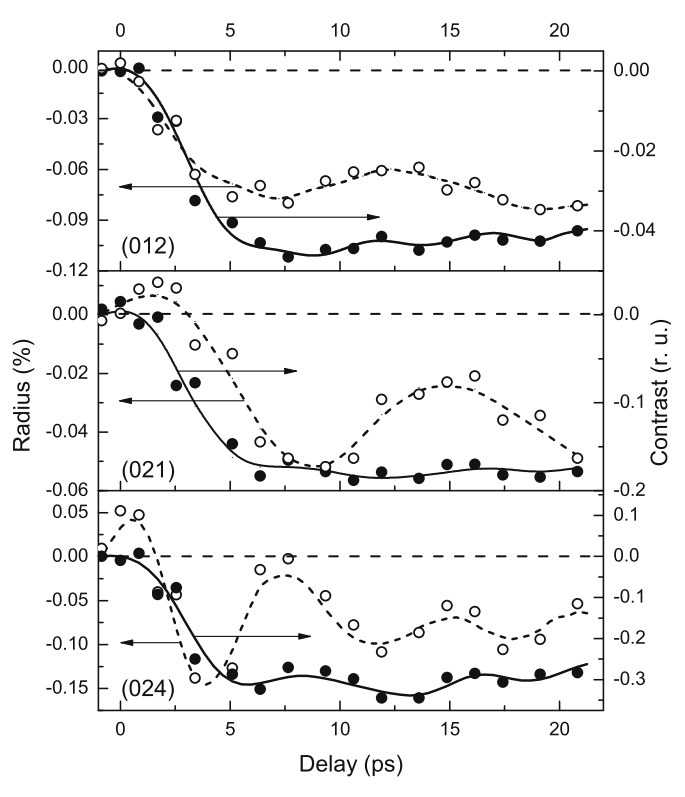


Fig. 2. Temporal dependence of the change in the radius $R(t) = (R(t) - R_0)/R_0$ in % (open circles) and intensity contrast $I(t) = (V(t) - V_0)/V_0$ (relative units) (closed circles) for diffraction orders of the bismuth film. Circles denote the experimental data and lines indicate the results obtained by low pass parabolic fast Fourier transform filtering of the data.

(021) and (024)). At a pump fluence of 1.5 mJ/cm², the amplitude of the positive peaks was proportional to the fluence and it indicated compression. The value of the lattice compression detected based on the positive change in the (024) ring radius was $\sim\!0.05\%.$ The magnitude of the compression was ~ 0.02 at a laser fluence of 0.6 mJ/cm². However, the (012) order of Bi did not exhibit contraction at any time, or its amplitude may have been sufficiently small not to be detected within the instrumental limitations. The film was predominantly [012] textured with some [021] grains, as shown by the relative strengths of the diffraction peaks in Fig. 1. The peak of this compressive force occurred at ~2 ps after excitation. The drop in the diffraction intensity started at 2.5 ps, which approximately corresponded to the electron-phonon energy transfer time. In addition, the I(t) and R(t) dependences for the (012) and (024) orders almost matched in time, whereas there was a ~ 2.5 ps lag in R(t) relative to I(t) for the (021) order. It should be noted that a lag of 1 ps was also reported by probing a germanium lattice by femtosecond time-resolved X-ray diffraction [15] and in a UED study of aluminum [16]. In the present study, we focused mainly on analyzing the temporal behavior of R(t). The dynamics of the contrast I(t) were analyzed in a previous study [10].

The R(t) for several diffraction orders of Bi exhibited initial compression, followed by expansion where coherent vibrations were observed around the expanded lattice, as shown in Fig. 2. The range probed for the reciprocal lattice vector was $1.8{\text -}3.9\,\text{Å}^{-1}$. To the best of our knowledge, the initial compressive peak arising after femtosecond pulse excitation (Fig. 2) has not been detected in previous time-resolved experiments that probed acoustic coherent phonons in Bi, Ge, Al, and InSb nanometer thickness films and in Ag nanoparticles [8,14–18]. The stress wave that causes lattice compression was previously observed in optical [19] and X-ray [20] experiments with rather thick samples (220 nm for As₂Te₃ and 2 μ m for GaAs). These experiments also observed coherent acoustic phonon propagation in the crystals. The laser

excitation produced a stressed thin surface layer of lattice expansion, which was responsible for driving a compression–expansion strain wave that propagated into the bulk. According to a previous model [19], coherent acoustic phonons are generated by a picosecond laser pulse when the laser absorption length is shorter than the film thickness, where the laser absorption results in a temperature rise, which is assumed to be instantaneous, and the temperature then remains constant over time. The temperature rise causes a strain at a layer near the surface where the laser energy is absorbed, which propagates away from the surface at the longitudinal sound velocity, thereby producing a stress pulse that bounces between the two surfaces of the thin film.

During the femtosecond laser interaction with solids, the initial lattice compression was experimentally observed [15–18] and modeled [21–23] based on the hot electron blast arising from the inhomogeneous distribution of the absorbed energy from the pump pulse over the probed region. The hot electron blast is the ultrafast deformation of the lattice produced during nonequilibrium heating when the electron temperature T_e is significantly higher than that of the lattice T_l . The blast force depends on the electron temperature and temperature gradient, where this force lasts for about 1.5 ps in gold [23]. The laser spot size on our samples was much larger than the laser skin depth in the samples, so a one-dimensional model of electron excitation was assumed, which resulted in a hot electron blast force along the sample normal, thereby leading to a pressure [15–18,21–23]:

$$P(\tau) = \frac{2}{3} C_{e0} T_e^2(\tau), \tag{1}$$

Where $C_{e0} = \pi^2 N k_B / 2T_F$ is the electron heat capacity, which we treated as a constant, k_B is Boltzmann's constant, N is the atom density, T_F is the Fermi temperature, and T_e is the electron temperature [23]. The electrons were assumed to be fully thermalized with each other and they reached their thermal Fermi-Dirac distribution in a time scale similar to that of the excitation laser pulse width. Hot electrons indicate an electron distribution that is out of equilibrium with the lattice. The blast force was generated from the gradient in T_e across the sample thickness, ∇T_e . In previous studies of the femtosecond excitation of metals (e.g. Ref. [16]), the electron heat capacity C_e was considered to be proportional to T_e , $C_e = C_{e0}T_e$. However, for the high laser fluences used in the present study, this assumption was inaccurate at a time scale below that of the electron-phonon relaxation time, which could affect the accuracy of the maximum calculated T_e and the magnitude of ∇T_e . The UED data based on changes in the diffraction radius were fitted to the model over a time period that extended to 20 ps, which was much longer than the electron-phonon relaxation time. Therefore, inaccuracies in the fit due to the assumption that C_e is proportional to T_e did not affect the values for the electron-phonon coupling time or the Grüneisen parameters obtained for the electronic subsystem. Failure to conform to this assumption would have affected the calculated value of T_e , which was not considered in the present study. For the 800-nm pump laser, the absorption coefficient of Bi was $\alpha_{Bi} \sim 7.10^5 cm^{-1}$ [24]. The laser energy initially absorbed into the sample decayed exponentially with the depth. The initial electron excitation (electron temperature and excitation density) decreased exponentially with the film depth because of the large absorption coefficient of Bi. Consequently, the gradient established in the pressure P(t) resulted in a hot electron blast force:

$$F_z(t,z) = \frac{\partial}{\partial z} P(t,z) = \frac{\partial}{\partial z} \left(\frac{2}{3} C_{e0} T_e^2(t,z) \right), \tag{2}$$

where F_z is the z-component of vector \bar{F} . Due to this gradient force, the compression stress σ_z was normal to the surface of the film. The electron pulse probed the thin film in the transmission mode. Therefore, the lattice parameters were observed in a region across the z-direction over the film thickness and the area of the electron pulse on the Bi thin film. The observed diffraction pattern was the superposition of the diffraction from the detected regions. The diffraction pattern exhibited

compression when more of the volume was compressed at a certain time over the detected region, whereas the diffraction pattern exhibited expansion when more of the volume was expanded. When the gradient in the electronic pressure was removed or reduced, the initial lattice compression disappeared. The origin of the lag in time between I(t) and R(t), which was mainly observed in the (021) order, was determined by the combined action of pulsed compression due to the electron blast force and thermal expansion. Depending on the amplitude and duration of the electron blast force, the resulting dependence of R(t) exhibited a lag. No lag appeared in any of the diffraction orders when the hot electron blast force was not included. The initial compression was not accompanied by a drop in the diffraction intensity because the reduction in the diffraction intensity was due to the electron–phonon coupling increasing the mean atomic vibrational amplitude.

For anisotropic materials such as Bi, the introduction of a stress in any direction causes strain in all directions [25], $\varepsilon_{ij} = S_{ijkl} \cdot \sigma_{kl}$ (where S_{ijkl} is a fourth-rank tensor). Consequently, the hot electron blast force F_z perpendicular to the surface of the sample also caused strains in the x–y plane.

The distribution of T_e across the film thickness became uniform due to electron transport and electron–phonon coupling. Therefore, the initially compressed state of the excited Bi film decayed over time. The driving force for the generation of acoustic phonons was represented by the combined transient thermal stresses [26] due to electronic σ_e and lattice σ_l heating, and the hot electron blast force:

$$\sigma(t,z) = \frac{1}{A} \frac{\partial}{\partial z} \left(\frac{2}{3} C_{e0} T_e^2(t,z) \right) - \gamma_e \int_{T_R}^{T_e} C_e dT_e(t,z) - \gamma_l \int_{T_R}^{T_l} C_l dT_l(t,z),$$
(3)

where C_e and C_l are the electron and phonon heat capacities, respectively, γ_e and γ_l are the Grüneisen parameters for the electrons and phonons, T_e and T_l are the electron and lattice temperatures, T_R is the room temperature, and A is the surface area. The hot electron distribution was generated almost instantly (the time period for an electron's temperature to reach equilibrium distribution is $\approx \frac{\varepsilon_F}{\omega_p \varepsilon_e} \sim 4$ fs, where ε_e is the energy of electrons excited above the Fermi level ε_F and ω_p is the plasma frequency [27]). Therefore, at the initial stage of excitation, the gradient blast force dominated the electronic and lattice heating terms. At room temperature, the electronic thermal Grüneisen parameter for Bi is expected to be positive in a similar manner to other elements with high atomic number [28].

The temporal dependence of the lattice vibrations shown in Fig. 2 was fitted to a classical simple damped harmonic oscillator model:

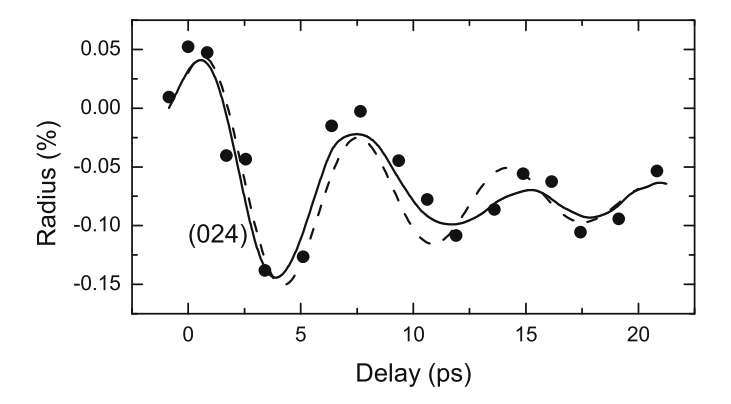
$$X'' + 2\beta X' + \omega_0^2 X = H\sigma(t), \tag{4}$$

where X (t) is the lattice displacement, H is a scaling factor, β and ω_0 are the damping constant and phonon angular frequency, respectively, and $\sigma(t)$ is the driving force. A detailed calculation of the electron blast force was previously derived from a solution of the Boltzmann transport equation [23,29]. After neglecting the temperature dependences of C_e and C_l , the thermal stress can be expressed in its known form [18,19,30]:

$$\sigma(t) = -\gamma_e C_e \Delta T_e(\tau) - \gamma_l C_l \Delta T_l(\tau)$$

$$= -\gamma_l E_T [(\gamma_e/\gamma_l) g(t) - (\gamma_e/\gamma_l - 1)(1 - \exp(-t/\tau_{e-ph}))], \tag{5}$$

where E_T is the total laser energy deposited per unit volume, g(t) is the normalized temporal profile of the laser pulse, and τ_{e-ph} is the electron–phonon energy exchange time. To consider the electron blast force, the initial conditions for Eq. (4) must satisfy $X(0) = a \ge 0$, and $X'(0) = b \ge 0$. These conditions simply state that at the maximum amplitude of the exciting laser pulse (t = 0), the atom can stay close to or leave the initial equilibrium position $(X(0) = a \ge 0)$ and it possesses a certain speed $(X'(0) \ge 0)$, which is caused by the compressing hot electron blast force. For Bi, which is highly anisotropic, one could



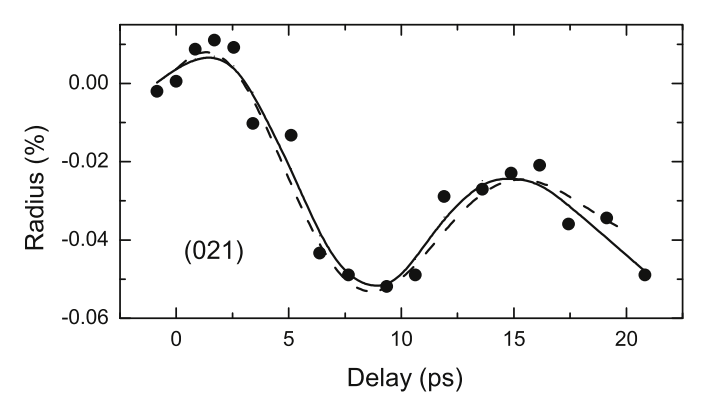


Fig. 3. Numerical fitting of the driven harmonic oscillator model (dashed lines) to the results obtained by low pass parabolic fast Fourier transform filtering (solid lines) of the experimental data (closed circles) for the changes in radius for the (024) and (021) diffraction orders.

expect that both of these conditions depend on the orientation of the vector X'(0) relative to the elongated body diagonal of the crystal [31,32]. In general, this means that the value of the derivative can contribute differently to various diffraction orders.

According to Nie et al. [30], based on the numerical fit of the solution of Eq. (4) to the experimental results, the following parameters were obtained: (i) electron-phonon energy exchange time τ_{e-ph} , (ii) ratio of Grüneisen parameters γ_e/γ_l , and (iii) angular frequency ω_0 . The fitting was limited to approximately 1.5-2 times the period of the oscillations because the structure of the oscillations degraded outside this time. This time can be considered as the coherent time of an acoustical phonon spectrum. Originally, these phonon modes were rigidly synchronized by the femtosecond pulse but the phase mismatch increased with time and the dependence departed from simple harmonic oscillation. Examples of the fits are shown in Fig. 3. The parameters retrieved from the fits are presented in Table 1 with the interplanar distance d from JCPDS Card No. 44–1246. Our results showed that τ_{e-ph} was strongly anisotropic where values of ~ 1.3 , ~ 1.4 , and ~ 2.2 ps corresponded to diffraction orders of (012), (024) and (021), respectively. Due to the convolution of the lattice response with the probe electron pulse width, the values obtained as $\sim 1.3 \,\mathrm{ps} \,(012)$ and

Table 1 Parameters obtained from diffraction orders (hkl) using the interplanar distance d, electron–phonon energy exchange rate τ_{e-ph} , ratio of the Grüneisen parameters γ_e/γ_l , and oscillation frequency ν .

(hkl)	d (Å)	$\tau_{e-ph}(ps)$	ν (GHz)	γ_e/γ_l
(012)	3.268	1.3	70	0.60
(021)	1.936	2.2	80	0.60
(024)	1.634	1.4	150	0.58

~ 1.4 ps (024) are the upper limits due to the temporal resolution of our UED setup. It should be noted that the value of $\tau_{e-ph} \sim 2.2$ ps obtained in our experiment corresponded well with the integrated value of the time constant for the rise in the inelastic scattering measured previously for Bi [9]. In addition, under our experimental conditions (excitation fluence ~1.5 mJ/cm²), the theoretical evaluations of the electron-phonon exchange rate [32,33], i.e., $\tau_{e-ph} \sim \frac{T_D^2 \varepsilon_F}{\hbar \omega_D^2 T_L^2} \sim (2-4)$ ps, yielded approximately the same range (T_D is the Debye temperature, ε_F is the Fermi level, \hbar is Plank's constant divided by 2π , ω_D is the Debye frequency, and T_L is the lattice temperature). Our results indicated the anisotropy of τ_{e-ph} in Bi, as observed in our previous studies [10,11]. Moreover, our results are strongly supported by previous detailed theoretical analyses of anisotropic relaxation-time tensors for materials with Fermi surfaces comprising a group of ellipsoids [34,35].

The previously measured linear thermal expansion of a single-crystal bismuth rod was used to determine γ_e , based on which the lattice Grüneisen parameters were calculated as $\gamma_\perp=1.32$ and $\gamma_{||}=1.1$, where the symbols || and \bot denote the parallel and perpendicular directions relative to the crystal's trigonal axis [36]. After neglecting the possible anisotropy of γ_e and using the average values for the γ_e/γ_l ratio derived from the experiment, we obtained $\gamma_e=0.72$. To the best of our knowledge, measured or theoretical values of the electronic Grüneisen parameter γ_e have not been reported previously for Bi. We consider that the value obtained for γ_e is only an estimate. We previously reported measurements of γ_e for Sb, which were obtained using the same experimental setup [37]. The results are similar because both elements have a rhombohedral structure and similar electronic properties.

The observed coherent phonon oscillations in R(t) occurred at frequencies of 70-150 GHz, which are excessively high for breathing modes and they could not exceed 64 GHz under our experimental conditions (maximum velocity of sound for Bi $v = 2.57 \,\mathrm{km/s}$ [38]). However, the observed oscillation frequencies were excessively low compared with the phonon frequencies measured in a Bi crystal by neutron inelastic scattering [39]. Previously, it was observed that in addition to the two main peaks for the optical phonons, i.e., the A_{1g} (2.78 THz) and E_g (2.2 THz) modes, four peaks could be attributed to acoustic phonons: TA(X) at 0.68 THz, LA(X) at 1.02 THz, LA(A) at 1.42 THz, and LA(T) at 1.76 THz [40]. The exact source of the observed oscillations at 70-150 GHz is not known. We previously suggested that these low frequency oscillations may be due to combinations of several phonons or confined acoustic phonon modes [10], as suggested for the low frequency broad-band peaks observed in the Raman spectra of nanocrystalline Bi [41]. For nanocrystals with a mean height of 6.18 nm and mean diameter of 23 \pm 2 nm, this broad-band was centered at ~500 GHz with a wing extending to < 100 GHz [41]. The Bi film investigated in the present study comprised grains with a mean thickness of 20-22 nm and the grain size distribution in the lateral dimensions was mostly in the order of several tens of nanometers according to the TEM observations. The vapor-deposited film contained many defects, including dislocations, staking faults, and grain boundaries. Thus, possible effects due to the grain size distribution, grain shape, and crystalline defects on acoustic phonon confinement for the observed oscillations at 70-150 GHz cannot be excluded. The amorphous carbon backing film could also have affected the damped frequency response of the film. The frequency of oscillation observed in the (012) diffraction order was about twice that observed for the (024) diffraction order. We note that the interplanar distance d for the (012) planes was twice that of the (024) planes, as shown in Table 1.

The influence of reflected light from the back surface of the film could be neglected because of the large absorption coefficient of the 800-nm laser in Bi [24]. The inhomogeneous optical excitation across the film thickness was the fundamental source of the electron blast force and it was included in the gradient of T_e . Based on the absorption coefficient of Bi, for the 800-nm light that penetrated the film (i.e., not

reflected at the Bi–air interface), only $\sim 20\%$ reached the Bi–C interface. The refractive index of Bi at 800 nm is 2.78 and that of graphite is 1.96, thereby resulting in $\sim 3\%$ reflection at the Bi–C interface [42]. Therefore, only $\sim 3\%$ of the 20% of the light that reached the Bi–C interface would have been reflected back. This value (0.6%) is excessively small to affect the dynamics.

The electronic Grüneisen parameter γ_e denotes the change in the dimensions of a solid due to the heating of its conduction electrons. The use of UED to probe γ_e at room temperature avoids complications associated with the need for low temperatures in the conventional techniques employed for measuring γ_e [30]. γ_e has been characterized by UED for only a few materials, i.e., Al, Ni, and Sb [30,37,43]. Measuring γ_e of Bi using low-temperature methods is particularly challenging because Bi exhibited high magnetoresistance [44]. The importance of characterizing the fundamental properties of Bi, such as γ_e , is due to its technologically important properties in terms of superconductivity [45] and its metal-to-semiconductor transition at a critical thickness [46], which make Bi a useful material for optical and electro-optical applications.

4. Summary

In this study, we used UED to detect the generation of coherent acoustic phonons after the femtosecond laser irradiation of bismuth film. The temporal development of both the intensity and angle of the diffraction orders were measured. An initial compressive peak was observed based on the change in the diffraction Bragg peak angle. The temporal development of the lattice spacing was described by a model based on a damped harmonic oscillator, which considered the effect of the hot electron blast force. According to the numerical fitting results, the energy exchange rates between the hot electrons and the phonons were determined as well as electronic Grüneisen parameters.

This study is based on research supported by the National Science Foundation under Grant No. 1708717.

References

- [1] Chong-Yu Ruan, Vigliotti Franco, Vladimir A. Lobastov, Songye Chen, Ahmed H. Zewail, Ultrafast electron crystallography: transient structures of molecules, surfaces, and phase transitions, Proc. Natl. Acad. Sci. Unit. States Am. (2014) 1123.
- [2] Ahmed H. Zewail, 4D Ultrafast electron diffraction, crystallography, and microscopy, Annu. Rev. Phys. Chem. 57 (2006) 65.
- [3] R.J. Dwayne Miller, Femtosecond crystallography with ultrabright electrons and X-rays: capturing chemistry in action, Science 343 (2014) 1108.
- [4] Anatoly A. Ischenko, Peter M. Weber, R.J. Dwayne Miller, Capturing chemistry in action with electrons: realization of atomically resolved reaction dynamics, Chem. Rev. 117 (2017) 11066.
- [5] S. Williamson, G. Mourou, J.C.M. Li, Time-resolved laser-induced phase transformation in aluminum, Phys. Rev. Lett. 52 (1984) 2364.
- [6] Peter Baum, Ding-Shyue Yang, Ahmed H. Zewail, 4D visualization of transitional structures in phase transformations, Science 318 (2007) 788.
- [7] Germán Sciaini, R J Dwayne Miller, Femtosecond electron diffraction: heralding the era of atomically resolved dynamics by Electron Diffraction, Rep. Prog. Phys. 74 (2011) 096101.
- [8] G. Sciaini, M. Hada, J. Matsuo, A. Karantza, G. Moriena, R.J. Dwayne Miller, Coherent acoustic phonons in highly oriented bismuth films monitored by femtosecond electron diffraction, International Conference on Ultrafast Phenomena, OSA Technical Digest (CD), Optical Society of America, 2010paper FA6.
- [9] G. Sciaini, M. Harb, S.G. Kruglic, T. Payer, C.T. Hebeisen, F.-J. Meyer zu Heringdorf, M. Yamaguchi, M. Horn-von Hoegen, R. Ernstofer, R.J. Dwayne Miller, Electronic acceleration of atomic motions and disordering in bismuth, Nature 458 (2009) 56.
- [10] A. Bugayev, A. Esmail, M. Abdel-Fattah, H.E. Elsayed-Ali, Coherent phonons in bismuth film observed by ultrafast electron diffraction, AIP Adv. 1 (2011) 012117.
- [11] A.R. Esmail, H.E. Elsayed-Ali, Anisotropic response of nanosized bismuth films upon femtosecond laser excitation monitored by ultrafast electron diffraction, Appl. Phys. Lett. 99 (2011) 161905.
- [12] H.E. Elsayed-Ali, 23rd international congress on high-speed photography and photonics, SPIE Proceedings 3516 (1998) 607.
- [13] B.-L. Qian, H.E. Elsayed-Ali, Electron pulse broadening due to space charge effects in a photoelectron gun for electron diffraction and streak camera systems, J. Appl. Phys. 91 (2002) 462.
- [14] V.M. Kaganer, R. Köhler, M. Schmidbauer, R. Opitz, B. Jenichen, X-ray diffraction

- peaks due to misfit dislocations in heteroepitaxial structures, Phys. Rev. B $55\ (1997)\ 1793$.
- [15] K. Sokolowski-Tinten, U. Shymanovich, M. Nicoul, J. Blums, A. Tarasevitch, M. Horn-von-Hoegen, D. von der Linde, A. Morak, T. Wietler, Energy relaxation and anomalies in the thermo-acoustic response of femtosecond laser-excited germanium, Chem. Phys. 88 (2007) 597.
- [16] H. Park, X. Wang, S. Nie, R. Clinite, J. Cao, Mechanism of coherent acoustic phonon generation under nonequilibrium conditions, Phys. Rev. B 72 (2005) 100301.
- [17] A.M. Lindenberg, I. Kang, S.L. Johnson, T. Missalla, P.A. Heimann, Z. Chang, J. Larsson, P.H. Bucksbaum, H.C. Kapteyn, H.A. Padmore, R.W. Lee, J.S. Wark, R.W. Falcone, Time-resolved X-ray diffraction from coherent phonons during a laser-induced phase transition, Phys. Rev. Lett. 84 (2000) 111.
- [18] M. Perner, S. Gresillon, J. Marz, G. von Plessen, J. Feldmann, J. Porstendorfer, K.-J. Berg, G. Berg, Observation of hot-electron pressure in the vibration dynamics of metal nanoparticles, Phys. Rev. Lett. 85 (2000) 792.
- [19] C. Thomsen, H.T. Grahn, H.J. Maris, J. Tauc, Surface generation and detection of phonons by picosecond light pulses, Phys. Rev. 34 (1986) 4129.
- [20] C. Rose-Petruck, R. Jimenez, T. Guo, A. Cavalleri, C.W. Siders, F. Raksi, J.A. Squier, B.C. Walker, K.R. Wilson, C.P.J. Barty, Picosecond–milliangström lattice dynamics measured by ultrafast X-ray diffraction, Nature 398 (1999) 310.
- [21] D.Y. Tzou, J.K. Chen, J.E. Beraun, Hot-electron blast induced by ultrashort-pulsed, lasers in layered media, Int. J. Heat Mass Tran. 45 (2002) 3369.
- [22] H. Wang, W. Dai, R. Nassar, R. Melnik, A finite difference method for studying thermal deformation in a thin film exposed to ultrashort-pulsed lasers, Int. J. Heat Mass Tran. 49 (2006) 2712.
- [23] J.K. Chen, D.Y. Tzou, J.E. Beraun, A semiclassical two-temperature model for ultrafast laser heating, Int. J. Heat Mass Tran. 49 (2006) 307.
- [24] H. Landolt, R. Bornstein, Condensed Matter, New Series, Group III 15 Pt Springer, New York, 2005 C.
- [25] J.F. Nye, Physical Properties of Crystals, Oxford University Press, Oxford, 2000.
- [26] G. Tas, H.J. Maris, Electron diffusion in metals studied by picosecond ultrasonics, Phys. Rev. B 49 (1994) 15046.
- [27] T. Garl, E.G. Gamaly, D. Boschetto, A.V. Rode, B. Luther-Davies, A. Rousse, Birth and decay of coherent optical phonons in femtosecond-laser-excited bismuth, Phys. Rev. B 78 (2008) 134302.
- [28] B.K. Godwal, Electronic thermal Gruneisen parameters for elements with high atomic number. J. Phys. F Met. Phys. 10 (1980) 377.
- [29] L.A. Falkovsky, E.G. Mishchenko, Electron-lattice kinetics of metals heated by ultrashort laser pulses, J. Exp. Theor. Phys. Lett. 88 (1999) 54.
- [30] Shouhua Nie, Xuan Wang, Hyuk Park, Richard Clinite, Jianming Cao, Measurement of the electronic Grüneisen constant using femtosecond electron diffraction, Phys. Rev. Lett. 96 (2006) 025901.
- [31] S. Epstein, A.P. deBretteville Jr., Elastic constants of and wave propagation in antimony and bismuth, Phys. Rev. 138 (1965) A771.
- [32] P. Fisher, I. Sosnowska, M. Szymanski, Debye-Waller factor and thermal expansion of arsenic, antimony and bismuth, J. Phys. C Solid State Phys. 11 (1978) 1043.
- [33] Yu A. Il'inskii, L.V. Keldysh, Electromagnetic Response of Material Media, Plenum, New York, 1994.
- [34] T.D. Fuchser, H.J. Mackey, J.R. Sybert, Anisotropic relaxation times and magnetoconductivity for ellipsoidal energy surfaces: onsager reciprocity restrictions and Jones-Zener expansions, Phys. Rev. B 2 (1970) 3863.
- [35] R. Hartman, Temperature dependence of the low-field galvanomagnetic coefficients of Bismuth, Phys. Rev. 181 (1969) 1070.
- [36] G.V. Bunton, S. Weintroub, The thermal expansion of antimony and bismuth at low temperatures, J. Phys. Chem. 2 (1969) 116.
- [37] Mahmoud Abdel-Fattah, Aleksey Bugayev, Hani E. Elsayed-Ali, Lattice dynamics of femtosecond laser-excited antimony, Physica B: Phys. Condens. Matter 492 (2016) 65–69.
- [38] Y. Eckstein, A.W. Lawson, D.H. Reneker, Elastic constants of bismuth, J. Appl. Phys. 31 (1960) 1534.
- [39] J.L. Yarnell, J.L. Warren, R.G. Wenzel, S.H. Koenig, Phonon dispersion curves in bismuth, IBM Technical Journals 8 (1964) 234.
- [40] A.Q. Wu, X. Xu, Coherent phonon excitation in bismuth, Appl. Surf. Sci. 253 (2007) 6301.
- [41] E. Haro-Poniatowski, M. Jouanne, J.F. Morhange, M. Kanehisa, Size effects investigated by Raman spectroscopy in Bi nanocrystals, Phys. Rev. B 60 (1999) 10 080
- [42] H.-J. Hagemann, W. Gudat, C. Kunz, Optical constants from the far infrared to the x-ray region: Mg, Al, Cu, Ag, Au, Bi, C, and Al₂O₃, J. Opt. Soc. Am. 65 (1975) 742–744.
- [43] Xuan Wang, Shouhua Nie, Junjie Li, Richard Clinite, Mark Wartenbe, Marcia Martin, Wenxi Liang, Jianming Cao, Electronic Grüneisen parameter and thermal expansion in ferromagnetic transition metal, Appl. Phys. Lett. 92 (2008) 121918.
- [44] F.Y. Yang, Kai Liu, Kimin Hong, D.H. Reich, P.C. Searson, C.L. Chien, Large magnetoresistance of electrodeposited single-crystal bismuth thin films, Science 284 (1999) 1335.
- [45] Y. Liu, K.A. Mcgreer, B. Nease, D.B. Haviland, G. Martinez, J.W. Halley, A.M. Geldman, Scaling of the insulator-to-superconductor transition in ultrathin amorphous Bi films, Phys. Rev. Lett. 67 (1991) 2068.
- [46] M.R. Black, P.L. Hagelstein, S.B. Cronin, Y.M. Lin, M.S. Dresselhaus, Optical absorption from an indirect transition in bismuth nanowires, Phys. Rev. B 68 (2003) 235417.